Article

Understanding cAMP-Dependent Allostery by NMR Spectroscopy: Comparative Analysis of the EPAC1 cAMP-Binding Domain in Its Apo and cAMP-Bound States

Mohammad T. Mazhab-Jafari, Rahul Das, Steven A. Fotheringham, Soumita SilDas, Somenath Chowdhury, and Giuseppe Melacini

J. Am. Chem. Soc., **2007**, 129 (46), 14482-14492• DOI: 10.1021/ja0753703 • Publication Date (Web): 31 October 2007

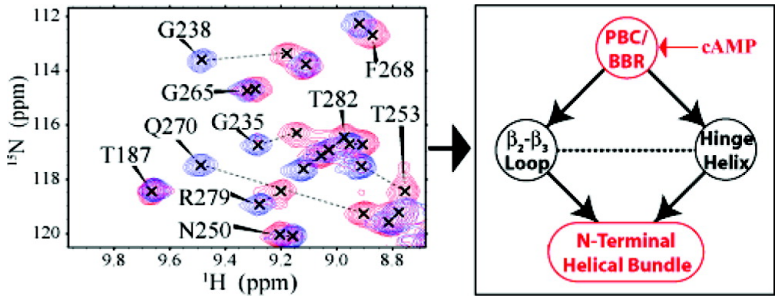

More About This Article

Additional resources and features associated with this article are available within the HTML version:

- Supporting Information
- Access to high resolution figures
- Links to articles and content related to this article
- Copyright permission to reproduce figures and/or text from this article

View the Full Text HTML

J|A|C|S
ARTICLES
Published on Web 10/31/2007

Understanding cAMP-Dependent Allostery by NMR Spectroscopy: Comparative Analysis of the EPAC1 cAMP-Binding Domain in Its Apo and cAMP-Bound States

Mohammad T. Mazhab-Jafari, Rahul Das, Steven A. Fotheringham, Soumita SilDas, Somenath Chowdhury, and Giuseppe Melacini*

Contribution from the Departments of Chemistry, Biochemistry and Biomedical Sciences, McMaster University, 1280 Main Street West, Hamilton, Ontario L8S 4M1, Canada

Received July 31, 2007; E-mail: melacin@mcmaster.ca

Abstract: cAMP (adenosine 3′,5′-cyclic monophosphate) is a ubiquitous second messenger that activates a multitude of essential cellular responses. Two key receptors for cAMP in eukaryotes are protein kinase A (PKA) and the exchange protein directly activated by cAMP (EPAC), which is a recently discovered guanine nucleotide exchange factor (GEF) for the small GTPases Rap1 and Rap2. Previous attempts to investigate the mechanism of allosteric activation of eukaryotic cAMP-binding domains (CBDs) at atomic or residue resolution have been hampered by the instability of the apo form, which requires the use of mixed apo/holo systems, that have provided only a partial picture of the CBD apo state and of the allosteric networks controlled by cAMP. Here, we show that, unlike other eukaryotic CBDs, both apo and cAMP-bound states of the EPAC1 CBD are stable under our experimental conditions, providing a unique opportunity to define at an unprecedented level of detail the allosteric interactions linking two critical functional sites of this CBD. These are the phosphate binding cassette (PBC), where cAMP binds, and the N-terminal helical bundle (NTHB), which is the site of the inhibitory interactions between the regulatory and catalytic regions of EPAC. Specifically, the combined analysis of the cAMP-dependent changes in chemical shifts, 2° structure probabilities, hydrogen/hydrogen exchange (H/H) and hydrogen/deuterium exchange (H/D) protection factors reveals that the long-range communication between the PBC and the NTHB is implemented by two distinct intramolecular cAMP-signaling pathways, respectively, mediated by the $\beta2-\beta3$ loop and the $\alpha6$ helix. Docking of cAMP into the PBC perturbs the NTHB inner core packing and the helical probabilities of selected NTHB residues. The proposed model is consistent with the allosteric role previously hypothesized for L273 and F300 based on site-directed mutagenesis; however, our data show that such a contact is part of a significantly more extended allosteric network that, unlike PKA, involves a tight coupling between the α- and β-subdomains of the EPAC CBD. The proposed mechanism of allosteric activation will serve as a basis to understand agonism and antagonism in the EPAC system and provides also a general paradigm for how small ligands control protein−protein interfaces.

Introduction

Cell-to-cell communication relies on the conversion of extracellular stimuli into tightly regulated intracellular responses. A key step in this transduction process is the relay of the external signals by second messengers, such as cAMP (adenosine 3′,5′-cyclic monophosphate). In mammals, two of the most important receptors for the cAMP second messenger are the ubiquitous cAMP-dependent protein kinase A (PKA) and the recently discovered exchange protein directly activated by cAMP (EPAC), which is a guanine-nucleotide-exchange factor (GEF) for the small GTPases Rap1 and Rap2.[1−5] Together, PKA and EPAC mediate the majority of cAMP responses, resulting in the regulation of a multitude of diverse cellular processes that range from ion-channel gating in the heart to insulin secretion in pancreatic β-cells, from memory development to cell growth, from cell adhesion to cell junction formation.[1−5]

The function of both PKA and EPAC is allosterically modulated by cAMP through conformational changes originating in their respective cAMP-binding domains (CBDs);[6] however, the understanding of the structural basis for the cAMP-dependent allostery in PKA and EPAC has been traditionally hampered by the instability of these CBDs in either the cAMP-bound or the apo states. For instance, the PKA CBDs are very stable and amenable to detailed structural investigations in their ligand-bound state,[7,8] but not in their apo form.[9] Conversely,

(1) Kawasaki, H.; Springett, G. M.; Mochizuki, N.; Toki, S.; Nakaya, M.; Matsuda, M.; Housman, D. E.; Graybiel, A. M. *Science* **1998**, *282*, 2275−2279.
(2) de Rooij, J.; Zwartkruis, F. J. T.; Verheijen, M. H. G.; Cool, R. H.; Nijman, S. M. B.; Wittinghofer, A.; Bos, J. L. *Nature* **1998**, *396*, 474−477.
(3) Bos, J. L. *Trends Biochem. Sci.* **2006**, *31*, 680−686.
(4) Kim, C.; Vigil, D.; Anand, G.; Taylor, S. S. *Eur. J. Cell Biol.* **2006**, *85*, 651−654.
(5) Bos, J. L. *Nat. Rev. Mol. Cell Biol.* **2003**, *4*, 733−738.
(6) Rehmann, H.; Wittinghofer, A.; Bos, J. L. *Nat. Rev. Mol. Cell Biol.* **2007**, *8*, 63−73.
(7) Su, Y.; Dostmann, W. R. G.; Herberg, F. W.; Durick, K.; Xuong, N. H.; Teneyck, L.; Taylor, S. S.; Varughese, K. I. *Science* **1995**, *269*, 807−813.

10.1021/ja0753703 CCC: $37.00

the EPAC CBDs have been crystallized in their apo state,[10,11] but their cAMP-bound form has remained so far largely elusive to high-resolution biophysical characterizations. A direct apo versus holo comparison for these CBDs at residue or atomic resolution is therefore not currently available.

For PKA, the experimental challenges arising from the instability of its apo form have been partially circumvented by exploiting an equilibrium perturbation approach, in which the apo state is stabilized by mixing it with large populations of cAMP-bound protein.[9] While this experimental strategy was instrumental to obtain an initial understanding of the cAMP-dependent allosteric mechanism in PKA,[12] it offered only a limited picture of the apo-state of mammalian CBDs. Furthermore, it is still not clear to what extent the model proposed for the cAMP-dependent control of PKA can be extended to EPAC. The low degree of sequence homology between the EPAC and PKA CBDs (Figure S1) as well as molecular modeling[13] and the differential responses of EPAC and PKA to point mutations and to cAMP modifications[13−15] consistently suggest that significant differences exist between the allosteric activation mechanisms of EPAC and PKA. Considering that EPAC-selective cAMP-agonists have been proposed as promising drug leads for the therapy of hypoinsulinaemia[5] and of Alzheimer's disease (AD),[16−18] the full characterization of the differences between EPAC and PKA is pivotal for the future exploitation of EPAC as a potential drug target.

Two homologous variants of cAMP-binding EPAC proteins are currently known, EPAC1 and EPAC2,[3] and both share a similar multidomain organization with an N-terminal regulatory region (RR) and a C-terminal catalytic region (CR) (Figure 1a).[3] In EPAC1, the RR contains a Disheveled-Egl-10-Pleckstrin (DEP) domain followed by a cAMP-binding domain (CBD), as shown in Figure 1a.[3] While the DEP motif controls membrane localization and its deletion does not affect the cAMP-dependent activation of EPAC,[19,20] the CBD plays a key role in the regulation of EPAC.[3] The EPAC1 CBD recognizes cAMP and allosterically propagates the cAMP signal to the catalytic region. Similarly to EPAC1, EPAC2 contains the DEP−CBD motifs (Figure 1a).[3] However, in EPAC2 the DEP domain is preceded by an additional CBD (Figure 1a), which does not alter EPAC auto-inhibition or cAMP binding to the other CBD.[3] Both EPAC1 and EPAC2 share a similar domain organization in the catalytic region (Figure 1a) with an N-terminal Ras exchange motif (REM), which serves as a connection domain between the RR and the CR, and a C-terminal CDC25-homology domain (CDC25HD), which implements the guanine-nucleotide-exchange function of EPAC.[3,5] Between the REM and the CDC25HD modules, EPAC2 contains a ubiquitin-like Ras-association (RA) domain (Figure 1a).[3,5]

The structure of EPAC2 in its apo (i.e., "auto-inhibited") state has been recently solved by X-ray crystallography,[10] revealing a "closed" overall conformation in which the regulatory region covers the CDC25HD domain and sterically hinders access of Rap proteins to the catalytic region. The apo EPAC2 structure has also unveiled that such inhibitory steric hindrance is secured by a group of salt bridges between the CDC25HD domain and a helical bundle at the N-terminus of the second CBD.[10] Such ionic interactions are spatially well clustered and are collectively referred to as "ionic latch" (IL).[10] While the recently solved structure of apo-EPAC2 has elucidated the mechanism of EPAC inhibition, it is still not clear how cAMP removes that inhibition and activates the catalytic domain. Mutational studies suggest that cAMP-binding to the CBD N-terminal to the REM domain disrupts the IL and causes an as yet uncharacterized allosteric perturbation within this CBD that displaces the regulatory region away from the catalytic region.[6] This displacement in turn opens the access of Rap proteins to the catalytic domain. While such a model is at the current stage only hypothetical, it does clearly point out that it is the cAMP-triggered allosteric conformational change of the CBD N-terminal to the REM domain that activates EPAC. Hence, this CBD represents the "central controlling unit" of EPAC.

Here, we show that it is possible to investigate how cAMP controls the critical EPAC CBD by isolating a construct, that is, the (149−305) segment of human EPAC1, which is stable and amenable to high-resolution nuclear magnetic resonance (NMR) characterization in both its apo and its cAMP-bound states under our experimental conditions. $EPAC1_h$ (149−305) spans the EPAC1 CBD (Figure 1b,c) and comprises sites previously shown to be critical for the cAMP-dependent activation of EPAC by site-directed mutagenesis.[6,10,11] These include not only the ionic latch (IL), but also the phosphate binding cassette (PBC) and the C-terminal hinge helix (i.e., α6), which has been proposed to be coupled to the PBC through an hydrophobic cluster formed by L273 and F300 (Figure 1c).[3,6,11]

Given the high degree of homology between EPAC 1 and 2 (Figure 1c), the apo EPAC1 CBD is anticipated to preserve the general secondary structure architecture typical of CBDs with a contiguous β-subdomain forming a well-defined eight-stranded jelly roll β-barrel and a noncontiguous all α-helical subdomain (Figure 1c,d).[10,11,21−34] Each subdomain contains a key functional region: the β-subdomain includes the PBC, where cAMP

(8) Wu, J.; Jones, J. M.; Xuong, N. H.; Ten Eyck, L. F.; Taylor, S. S. *Biochemistry* **2004**, *43*, 6620−6629.
(9) Das, R.; Abu-Abed, M.; Melacini, G. *J. Am. Chem. Soc.* **2006**, *128*, 8406−8407.
(10) Rehmann, H.; Das, J.; Knipscheer, P.; Wittinghofer, A.; Bos, J. L. *Nature* **2006**, *439*, 625−628.
(11) Rehmann, H.; Prakash, B.; Wolf, E.; Rueppel, A.; de Rooij, J.; Bos, J. L.; Wittinghofer, A. *Nat. Struct. Biol.* **2003**, *10*, 26−32.
(12) Das, R.; Esposito, V.; Abu-Abed, M.; Anand, G. S.; Taylor, S. S.; Melacini, G. *Proc. Natl. Acad. Sci. U.S.A.* **2007**, *104*, 93−98.
(13) Dao, K. K.; Teigen, K.; Kopperud, R.; Hodneland, E.; Schwede, F.; Christensen, A. E.; Martinez, A.; Doskeland, S. O. *J. Biol. Chem.* **2006**, *281*, 21500−21511.
(14) Rehmann, H.; Schwede, F.; Doskeland, S. O.; Wittinghofer, A.; Bos, J. L. *J. Biol. Chem.* **2003**, *278*, 38548−38556.
(15) Christensen, A. E.; Selheim, F.; de Rooij, J.; Dremier, S.; Schwede, F.; Dao, K. K.; Martinez, A.; Maenhaut, C.; Bos, J. L.; Genieser, H. G.; Doskeland, S. O. *J. Biol. Chem.* **2003**, *278*, 35394−35402.
(16) McPhee, I.; Gibson, L. C. D.; Kewney, J.; Darroch, C.; Stevens, P. A.; Spinks, D.; Cooreman, A.; MacKenzie, S. J. *Biochem. Soc. Trans.* **2005**, *33*, 1330−1332.
(17) Maillet, M.; Robert, S. J.; Cacquevel, M.; Gastineau, M.; Vivien, D.; Bertoglio, J.; Zugaza, J. L.; Fischmeister, R.; Lezoualc'h, F. *Nat. Cell Biol.* **2003**, *5*, 633−U36.
(18) Robert, S.; Maillet, M.; Morel, E.; Launay, J. M.; Fischmeister, R.; Mercken, L.; Lezoualc'h, F. *FEBS Lett.* **2005**, *579*, 1136−1142.
(19) de Rooij, J.; Rehmann, H.; van Triest, M.; Cool, R. H.; Wittinghofer, A.; Bos, J. L. *J. Biol. Chem.* **2000**, *275*, 20829−20836.
(20) Qiao, J. B.; Mei, F. C.; Popov, V. L.; Vergara, L. A.; Cheng, X. D. *J. Biol. Chem.* **2002**, *277*, 26581−26586.
(21) (a) Berman, H. M.; Ten Eyck, L. F.; Goodsell, D. S.; Haste, N. M.; Kornev, A.; Taylor, S. S. *Proc. Natl. Acad. Sci. U.S.A.* **2005**, *102*, 45−50. (b) Yu, S. N.; Fan, F. H.; Flores, S. C.; Mei, F.; Cheng, X. D. *Biochem.* **2006**, *45*, 15318−15326.
(22) Rehmann, H.; Rueppel, A.; Bos, J. L.; Wittinghofer, A. *J. Biol. Chem.* **2003**, *278*, 23508−23514.
(23) Kraemer, A.; Rehmann, H. R.; Cool, R. H.; Theiss, C.; de Rooij, J.; Bos, J. L.; Wittinghofer, A. *J. Mol. Biol.* **2001**, *306*, 1167−1177.
(24) Qiao, J.; Mei, F.; Cheng, X. *Mol. Biol. Cell* **2002**, *13*, 431A−431A.
(25) Weber, I. T.; Steitz, T. A. *J. Mol. Biol.* **1987**, *198*, 311−326.
(26) Passner, J. M.; Schultz, S. C.; Steitz, T. A. *J. Mol. Biol.* **2000**, *304*, 847−859.

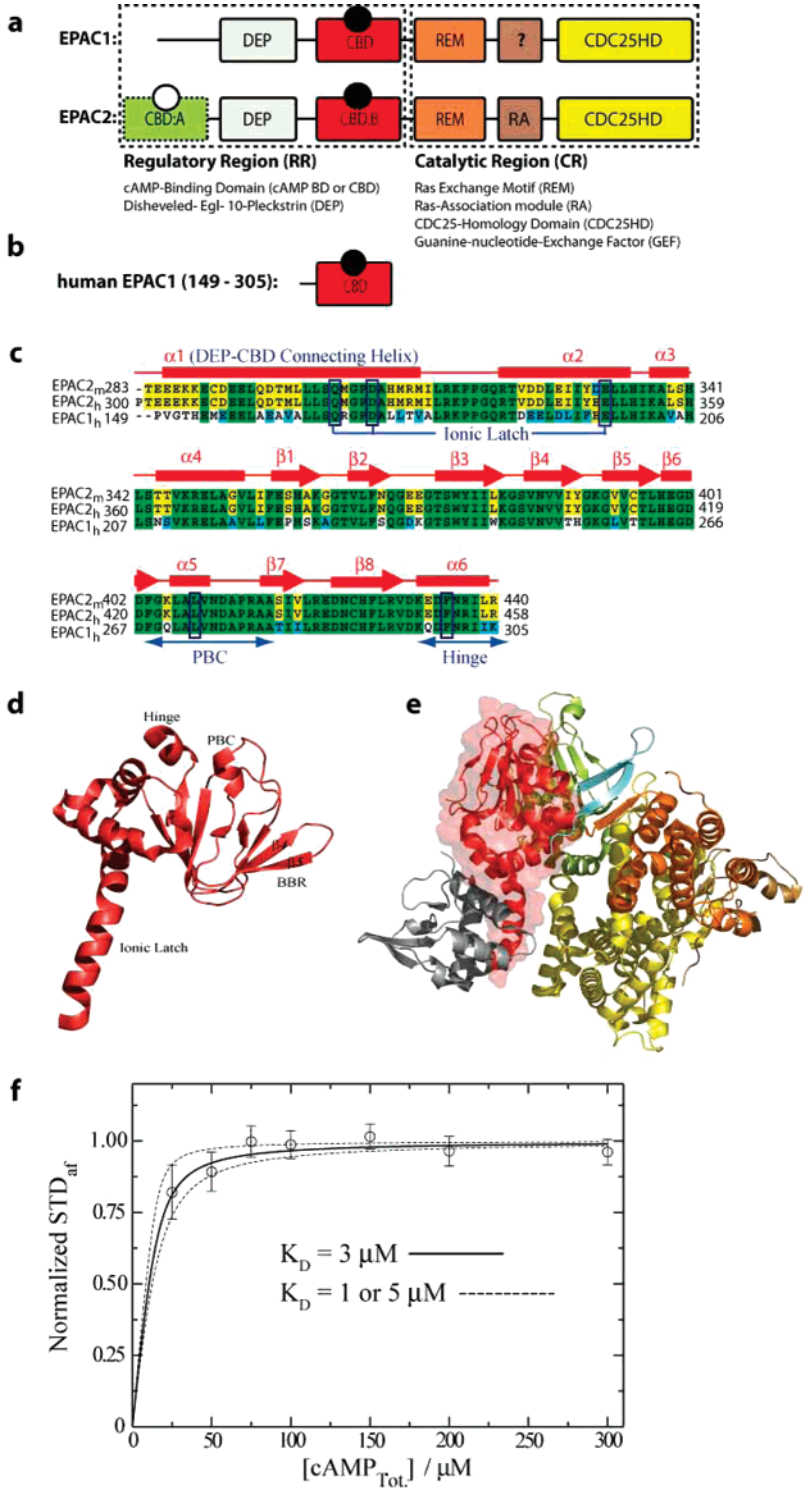

Figure 1. (a) Domain organization in human EPAC1 and EPAC2. The cAMP ligand is shown as a black circle. The CBD:A of EPAC2 is shown with a dotted contour and an empty cAMP circle meaning that such domain is not required for the regulation of EPAC2.[6] The EPAC1 segment homologous to the EPAC2 RA domain is currently functionally uncharacterized and is therefore labeled with a question mark.[6] Domain abbreviations are reported in the figure. (b) The human EPAC1 (149−305) construct employed for the NMR investigation presented here. This EPAC segment spans the DEP−CBD connecting helix and the CBD. (c) Sequence alignment of CBDs in human EPAC 1 ($EPAC1_h$), human EPAC2 ($EPAC2_h$), and mouse EPAC2 ($EPAC2_m$). The location of α-helices and β-strands, represented as red rectangles and arrows, respectively, was inferred from the crystal structure of apo $EPAC2_m$ (PDB accession code: 1O7F).[10] Strictly conserved residues in all three sequences are highlighted in green, while residues that are identical only in two of the three sequences are marked in yellow. Residues conserved only in terms of side-chain type are highlighted in cyan. Residues that are critical for the allosteric control of the EPAC CBD based on earlier mutational analyses[11] or on the apo-$EPAC2_m$ structure[10] are boxed within blue rectangles. (d) Ribbon diagram of apo-$EPAC2_m$ (291−440).[10] (e) Ribbon diagram of full-length apo-$EPAC2_m$[10] showing the van der Waals surface of the domain investigated here by NMR in the context of the other modules of this system. The color coding is as in panel (a) with the exception of the first two strands of the switchboard region,[10] which are shown in cyan. (f) Titration curve of cAMP into an NMR sample with 15 μM $EPAC1_h$ (149−305) in 20 mM phosphate buffer, pH 7.6, 50 mM NaCl, 99.9% D_2O, and at 25 °C. The binding of cAMP to $EPAC1_h$ (149−305) is monitored through the STD amplification factor (STD_{af}) normalized to the plateau value and plotted versus the total cAMP concentration. The solid line represents the binding isotherm corresponding to a K_D of 3 μM, while the dashed lines correspond to K_D values of 1 and 5 μM.

binds, while the α-subdomain encloses the IL (Figure 1c,d), where the catalytic and regulatory regions interact (Figure 1d,e). The PBC and the IL are far removed from each other in the EPAC structure (Figure 1d).[10] For the purpose of understanding how the cAMP-signal propagates from the PBC to the IL, we have analyzed the changes in chemical shifts, secondary structure, and hydrogen-exchange (H/D and H/H) protection factors caused by cAMP-binding to $EPAC1_h$ (149−305). Our NMR-based results reveal that the previously hypothesized hydrophobic hinge cluster involving L273 and F300 is part of a significantly more extended cAMP-dependent chain of interactions, mediating the cross-talk between the PBC and the IL through pathways relayed not only by the hinge helix but also by other critical allosteric "hot-spots" located within the *β*-subdomain. We have also identified striking differences between the CBDs of PKA and EPAC at the level of their N-terminal helical bundles.

Materials and Methods

Sample Preparation. The clone for $EPAC1_h$ (149−305) was prepared by inserting two stop codons into the pGEX-4T3 expression vector for $EPAC1_h$ (149−881) as a GST-fusion protein under the control of the *lac* promoter. The expression and purification of $EPAC1_h$ (149−305) was based on previously established protocols.[11] In brief, the *E. coli* strain BL21(DE3) was transformed with the plasmid for $EPAC1_h$ (149−305) and used for overexpressing the protein. Overexpression of isotopically enriched proteins was conducted with minimal media supplemented with trace metals, vitamins (10 μg/L thiamine and biotin), salts (NaCl, KH_2PO_4, and Na_2HPO_4), 1 g/L ^{15}N-ammonium chloride, 100 μg/mL ampicillin, and 3 g/L $^{12/13}$C-glucose for single- or double-labeled protein samples, respectively. The cultures were grown at 37 °C until an $O.D_{600}$ of 0.6 was reached, followed by induction with 1 mM IPTG for 3 h at 37 °C. Cells were harvested by centrifugation for 10 min at 8000*g* and 4 °C. The pellets were then resuspended in lysis buffer (PBS, 10 mM EDTA, 10% v/v glycerol) supplemented with protease inhibitors. The cells were lysed by passage through an EmulsiFlex-C5 homogenizer (AVESTIN) at 5000 PSI followed by centrifugation at 14 000*g* for 40 min. The supernatant was separated and incubated with pre-equilibrated Glutathione SepharoseT 4 Fast Flow beads (Amersham Biosciences, Inc.) with rotation for 4 h at 4 °C. The beads were washed with 0.5 M NaCl in 50 mM Tris, pH 8 and the expressed protein was cleaved from the GST tag using biotinylated thrombin. The thrombin was removed by incubation with Streptavidin beads, and further purification was achieved by ion exchange chromatography using a Q-column (GE Health Sciences). The protein was then dialyzed against the NMR buffer (50 mM HEPES at pH 7.6, 50 mM NaCl, 1 mM TCEP, 0.02% w/v NaN_3), and 5% v/v D_2O was added for the NMR measurements.

NMR Measurements. All NMR experiments were carried out at 34 °C on a Bruker AV 700 spectrometer equipped with a TCI cryoprobe. The temperature was calibrated with both a thermocouple and an ethylene glycol sample. The heteronuclear single-quantum coherence (HSQC) spectral widths were 31.8 and 14.2 ppm for the ^{15}N and ^{1}H dimensions, respectively, with 128 (^{15}N) and 1024 (^{1}H) complex points. The carrier frequencies of the proton and nitrogen channels were centered on the H_2O resonance and on the middle of the amide region, respectively. Proton chemical shifts were referenced relative to DSS, and the nitrogen dimension was then indirectly referenced using the nitrogen to proton gyro-magnetic ratio. For ^{15}N decoupling, we used the GARP4 pulse train with a 1.32 kHz radio frequency pulse (RF) strength. The resulting spectra were processed with both Xwinnmr (Bruker, Inc.) and NMRPipe.[35] Cross-peak fit heights were measured using Sparky[36] and Gaussian line fitting, unless otherwise specified. The assignments of the cAMP-bound and free states of $EPAC1_h$ (149−305) were obtained through a combination of classical triple resonance experiments:[37] HNCO, HNCA, HN(CO)CA, CBCA(CO)NH, HBHA(CO)NH, HNCACB, and HNHAHB. All 3D spectra were processed with NMRPipe[35] and analyzed using Sparky.[36] The secondary structure probabilities were obtained from the secondary chemical shifts using the PECAN program.[38] Compounded chemical shift differences between the cAMP-bound and free states of $EPAC1_h$ (149−305) were computed using the following formula:[39] $\Delta\delta_{compound} = ((\Delta\delta^1H)^2 + (\Delta\delta^{15}N/6.5)^2)^{0.5}$, where $\Delta\delta^1H$ and $\Delta\delta^{15}N$ are the differences between the proton and nitrogen chemical shifts of the apo and bound states, respectively.

H/D Exchange. H/D exchange experiments were performed on 0.25 mM U−^{15}N $EPAC1_h$ (149−305) prepared by 10× dilution with a 99.9% D_2O NMR buffer of a 2.5 mM sample in the H_2O NMR buffer (50 mM HEPES, 50 mM NaCl, 1 mM TCEP, and 0.02% w/v NaN_3). The dead-time of the experiment, defined as the time elapsed between the first exposure to D_2O and the start of the first HSQC, was ∼20 min. The H/D exchange rates were measured by a total of 84 HSQCs, in which the first 30 spectra accumulated only two scans and the remaining 64 spectra four scans. The total time of acquisition was 13 h. However, the peak intensity of the slowly exchanging amides was monitored for several days after D_2O exposure. The resulting cross-peak intensities were analyzed using NMRPipe[35] by employing a 3 × 3 matrix centered at each peak maximum. Errors on the cross-peak intensities were calculated using the standard deviation of the spectral noise. The rates of exchange were measured using the Levenberg−Marqardt nonlinear least-square exponential fitting implemented through the Curvefit software.[40] To calculate the errors for the exchange rates, we used the covariance matrix and Monte Carlo Simulation methods.[41] Alanine polypeptides were used as a base for the calculation of the intrinsic exchange rates using the program SPHERE.[42,43] The protection factors were computed as the ratios of the intrinsic to the observed exchange rates.

H/H Exchange. H/H exchange rates were measured using the CLEANEX-PM-FHSQC pulse sequence[44,45] and 0.2 mM U−^{15}N $EPAC1_h$ (149−305) with and without 2 mM excess cAMP. Mixing times of 5, 10, 20, 30, 40, and 60 ms were used for the calculation of the exchange rates. 32 scans were acquired per serial file with a 2 s inter-scan delay and an RF of 6.9 kHz for the CLEANEX-PM mixing

(27) Lawson, C. L.; Swigon, D.; Murakami, K. S.; Darst, S. A.; Berman, H. M.; Ebright, R. H. *Curr. Opin. Struct. Biol.* **2004**, *14*, 10−20.
(28) Napoli, A. A.; Lawson, C. L.; Ebright, R. H.; Berman, H. M. *J. Mol. Biol.* **2006**, *357*, 173−183.
(29) Chen, S. F.; Vojtechovsky, J.; Parkinson, G. N.; Ebright, R. H.; Berman, H. M. *J. Mol. Biol.* **2001**, *314*, 63−74.
(30) Chen, S. F.; Gunasekera, A.; Zhang, X. P.; Kunkel, T. A.; Ebright, R. H.; Berman, H. M. *J. Mol. Biol.* **2001**, *314*, 75−82.
(31) Kim, C.; Xuong, N. H.; Taylor, S. S. *Science* **2005**, *307*, 690−696.
(32) Dai, J. Y.; Lin, S. H.; Kemmis, C.; Chin, A. J.; Lee, J. C. *Biochemistry* **2004**, *43*, 8901−8910.
(33) Gekko, K.; Obu, N.; Li, J. Q.; Lee, J. C. *Biochemistry* **2004**, *43*, 3844−3852.
(34) Li, J. Q.; Cheng, X. D.; Lee, J. C. *Biochemistry* **2002**, *41*, 14771−14778.
(35) Delaglio, F.; Grzesiek, S.; Vuister, G. W.; Zhu, G.; Pfeifer, J.; Bax, A. *J. Biomol. NMR* **1995**, *6*, 277−293.
(36) Goddard, T. D.; Kneller, D. G. *SPARKY 3*; University of California, San Francisco.
(37) Sattler, M.; Schleucher, J.; Griesinger, C. *Prog. Nucl. Magn. Reson. Spectrosc.* **1999**, *34*, 93−158.
(38) Eghbalnia, H. R.; Bahrami, A.; Wang, L. Y.; Assadi, A.; Markley, J. L. *J. Biomol. NMR* **2005**, *32*, 219−233.
(39) Mulder, F. A. A.; Schipper, D.; Bott, R.; Boelens, R. *J. Mol. Biol.* **1999**, *292*, 111−123.
(40) Curvefit Copyright (C) 1998. Palmer, A. G. Department of Biochemistry and Molecular Biophysics, Columbia University, 630 West 168th Street, New York, NY 10032.
(41) Eckhardt, R.; Ulam, S.; von Neumann, J. *Los Alamos Sci.* **1987**, *15*, 131−137.
(42) Bai, Y. W.; Milne, J. S.; Mayne, L.; Englander, S. W. *Proteins: Struct., Funct., Genet.* **1993**, *17*, 75−86.
(43) Zhang, Y. Z. Ph.D. Thesis. Structural Biology and Molecular Biophysics, University of Pennsylvania, 1995.
(44) Hwang, T. L.; van Zijl, P. C. M.; Mori, S. *J. Biomol. NMR* **1998**, *11*, 221−226.
(45) Huang, H.; Melacini, G. *Anal. Chim. Acta* **2006**, *564*, 1−9.

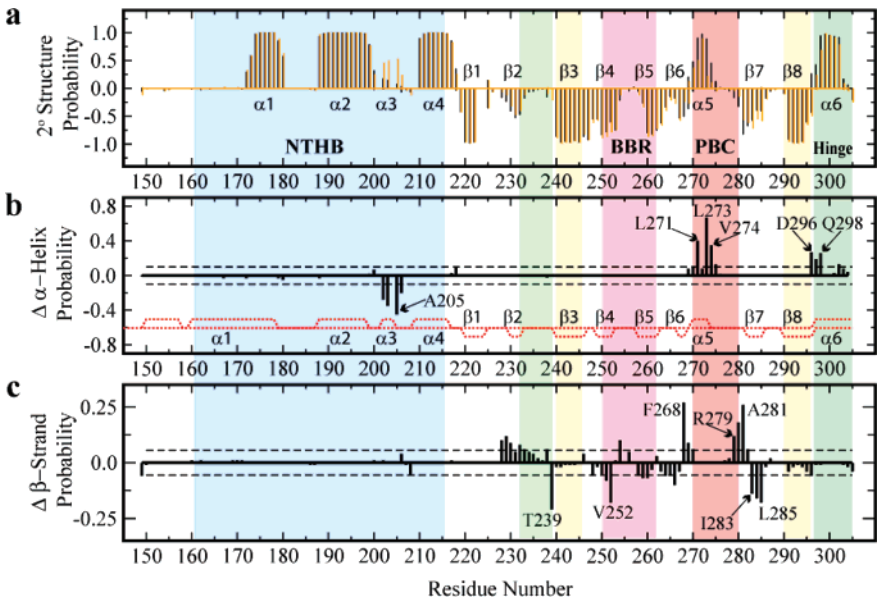

Figure 2. Plots of the residue-specific secondary structure probabilities for EPAC1$_h$ (149−305) based on the secondary chemical shifts. (a) Secondary structure probabilities of cAMP-bound (black) and apo (orange) EPAC1$_h$ (149−305) under the experimental conditions reported in the Materials and Methods section. Extended β-strand probabilities are reported as negative values, whereas α-helix probabilities are positive. NTHB stands for N-terminal helical bundle. (b) Differences between the α-helix probabilities of cAMP-bound and apo EPAC1$_h$ (149−305) reported in panel (a). Positive values indicate higher α-helix probability in the cAMP-bound form relative to the apo state. The dashed lines correspond to the mean of the α-helix probability variation distribution ± one standard deviation. Representative residues with significant cAMP-dependent α-helix probability variations are labeled. The secondary structure shown with red dotted lines was inferred as in Figure 1c. (c) Differences between the β-strand probabilities of cAMP-bound and apo EPAC1$_h$ (149−305) reported in panel (a). Positive values indicate higher extended β-strand probability in the cAMP-bound form relative to the apo state. The dashed lines correspond to the mean of the β-strand probability variation distribution ± one standard deviation. Critical functional regions are color-coded as follows: N-terminal helical bundle (blue), $\beta2-\beta3$ loop and α6 (light and dark green, respectively), $\beta3$ and $\beta8$ (beige), $\beta4-\beta5$ and PBC (pink). Representative residues with significant cAMP-dependent β-strand probability variations are labeled.

block. The measured CLEANEX-PM-FHSQC cross-peak heights were normalized according to the corresponding reference FHSQC cross-peak heights. The normalized build-up curves were analyzed as previously described.[44] The H/H-exchange-based protection factors were computed using the intrinsic rates calculated by the SPHERE software with H_2O as solvent and alanine polypeptides.

Sequence and Structure Analyses. Sequences were aligned using CLUSTALW,[46] and the structural model for EPAC1$_h$ (149−305) was obtained using the JIGSAW homology modeling software[47−49] based on the crystal structure of EPAC2$_m$[10] as template. Structures were analyzed using Pymol.[50] All solvent-accessible surface area (SASA) values were calculated using the Naccess program with a probe size of 1.4 Å.[51]

Binding Measurements. The dissociation constant (K_D) for the cAMP:EPAC1$_h$ (149−305) complex was measured using the saturation transfer difference (STD) amplification factor (STD$_{af}$) method, which has been previously shown to be suitable for the quantification of K_D values in the micromolar range for lectin/carbohydrate systems.[52] All STD measurements were carried out using a solution of 15 μM EPAC1$_h$ (149−305) in 20 mM phosphate buffer, pH 7.6, 50 mM NaCl, 99.9% D_2O, and at 25 °C. The 1D-STD spectra were acquired at total cAMP concentrations of 25, 50, 75, 100, 150, 200, and 300 μM and were implemented as described earlier,[52] using a selectively saturating train of 40 Gaussian-shaped pulses of 50 ms each separated by a 1 ms inter-pulse delay and a 60 ms spin-lock filter to minimize interferences from protein signals to the cAMP resonances. The strength of each Gaussian pulse was 119 Hz with a 1% truncation and 1000 digitization points. The train of Gaussian pulses was preceded by a 100 ms delay in all STD experiments. The spectral width was 8389.26 Hz and was digitized by 8 K complex points. The on-resonance irradiation was performed at 0.63 ppm, resulting in good signal-to-noise ratios even at low cAMP concentrations (Figure S2c), while avoiding direct saturation of the cAMP resonances (Figure S2a,b). The off-resonance control irradiation was at 30 ppm. The saturation transfer difference (STD) spectrum was obtained by phase cycling subtraction of the on-resonance and off-resonance data acquired in interleaved mode. The number of scans and dummy scans in the 1D-STD experiments was 512 and 8, respectively. Separate reference 1D-ST (saturation transfer reference, STR) experiments were also acquired with 128 scans and 8 dummy scans. The STD amplification factor (STD$_{af}$) was computed as the product of the STD/STR ratio, measured for the well-resolved cAMP ribose H1′ singlet at 6.2 ppm, and of the ratio of the total cAMP and protein concentrations.[52] The STD$_{af}$ values were then normalized relative to the STD$_{af}$ plateau value reached at high cAMP concentrations (i.e., [cAMP$_{Tot.}$] ≥ 150 μM). The normalized STD$_{af}$ values were then analyzed using the binding isotherm equation: normalized STD$_{af}$ = 1 − (1/(1 + ([cAMP]/K_D))), where [cAMP] is the concentration of free cAMP.[52]

Results

Secondary Structure Profiles of Apo and cAMP-Bound EPAC1$_h$ (149−305). The chemical shift-based secondary structure probabilities for EPAC1$_h$ (149−305) in its apo and cAMP-bound states are shown in Figure 2a. The secondary structure patterns observed for the CBD spanned by the apo EPAC1$_h$ (149−305) construct (i.e., residues 188−305) are in overall good agreement with the α/β fold of the corresponding CBD in the crystal structure of full-length apo EPAC[10] (Figure

(46) Thompson, J. D.; Higgins, D. G.; Gibson, T. J. *Nucleic Acids Res.* **1994**, *22*, 4673−4680.
(47) Bates, P. A.; Sternberg, M. J. E. *Proteins: Struct., Funct., Genet.* **1999**, 47−54.
(48) Contreras-Moreira, B.; Bates, P. A. *Bioinformatics* **2002**, *18*, 1141−1142.
(49) Gerstein, M.; Levitt, M. *Proc. Fourth Int. Conf. Int. Syst. Mol. Biol.* **1996**, 59−67.
(50) DeLano, W. *The PyMOL Molecular Graphics System*; CA De Lano Scientific: San Carlos, 2002.
(51) Hubbard, S. J.; Campbell, S. F.; Thornton, J. M. *J. Mol. Biol.* **1991**, *220*, 507−530.
(52) Stockman, B. J.; Dalvit, C. *Prog. Nucl. Magn. Reson. Spectrosc.* **2002**, *41*, 187−231.

2a). The N-terminal α1 helix that precedes the CBD (Figure 1c) and connects it to the DEP domain in full-length EPAC is largely unstructured in EPAC1$_h$ (149−305) (residues 150−187 in Figure 2a). Such a destabilization of helix α1 is explained by the absence of the N-terminal DEP domain, which in full-length EPAC interacts directly with the α1 helix.[10] However, deletion of the DEP domain at the CBD N-terminus (Figure 1a) has been shown to have a negligible effect on the cAMP-dependent activation of EPAC,[19,20] and therefore the resulting destabilization of the α1 helix is not expected to alter the functional relevance of the EPAC1$_h$ (149−305) construct, which provides a useful model system to evaluate the effect of cAMP-binding. This is confirmed by the dose−response curve for cAMP-binding monitored through the STD amplification factor (Figure 1f), showing that the affinity of EPAC1$_h$ (149−305) for cAMP is comparable to that previously reported for full-length EPAC1$_h$ (K_D = 2.9 μM).[13]

Figure 2a shows also that, while the global secondary structure profiles for cAMP-bound EPAC1$_h$ (149−305) remain quite similar to those observed for the apo-state, several local differences are observed upon cAMP-binding. The most significant variations in secondary structure probabilities are detected for the α-helices (Figure 2b), with both α5 and α6 being stabilized by cAMP, whereas the opposite effect is observed for α3 (Figure 2b). More subtle yet significant cAMP-dependent variations are measured for the β-strands (Figure 2c), with the regions of β6 and β7 adjacent to the phosphate binding cassette (PBC) being stabilized, while selected residues of β3, β4, and β7 are destabilized by cAMP (Figure 2c).

Chemical Shift Map of cAMP-Binding to EPAC1$_h$ (149−305). The ^{15}N,^{1}H compounded chemical shift variations (Figure 3a) are a sensitive probe of the effect of cAMP-binding to the EPAC CBD. The most significant variations are confined to the β-barrel (Figure 3b), and within the β-subdomain the most dramatic cAMP-dependent perturbations map well to the PBC (i.e., residues ∼270−280, Figure 3b−d). The other β-subdomain "hot-spots" revealed by the chemical shift plot cluster within the β2,β3 loop and in the β4−β5 region (Figure 3b). For the α-subdomain, the largest compounded chemical shift changes are observed for the C-terminal α6 helix (i.e., residues 297, 300, 303, and 305, Figure 3b). Most of these α6 chemical shift variations map to residues in the inner side of α6, which faces the β-barrel and the N-terminal helical bundle (Figure 3c,d).

Hydrogen-Exchange Profiles of Apo and cAMP-Bound EPAC1$_h$ (149−305). Hydrogen-exchange rates are a sensitive probe of the native state ensemble, providing unique insight not only on largely populated conformers but also on excited and at least partially unfolded states of proteins. In addition, the exchange-rate based protection factors (PFs) are directly related to the free energy variations associated with transitions to exchange-competent states, and therefore PFs are instrumental to map the free energy landscape of proteins and their dependence on ligand-binding.[9,12] Hydrogen-exchange rates are often measured at residue resolution by H/D NMR through real-time monitoring of deuterium incorporation; however, the H/D decay for the amides that are fully exchanged within the dead-time of the H/D experiment (∼20 min) cannot be quantified. For these fast exchanging amides, H/H exchange pulse sequences are very useful as they probe hydrogen-exchange processes occurring

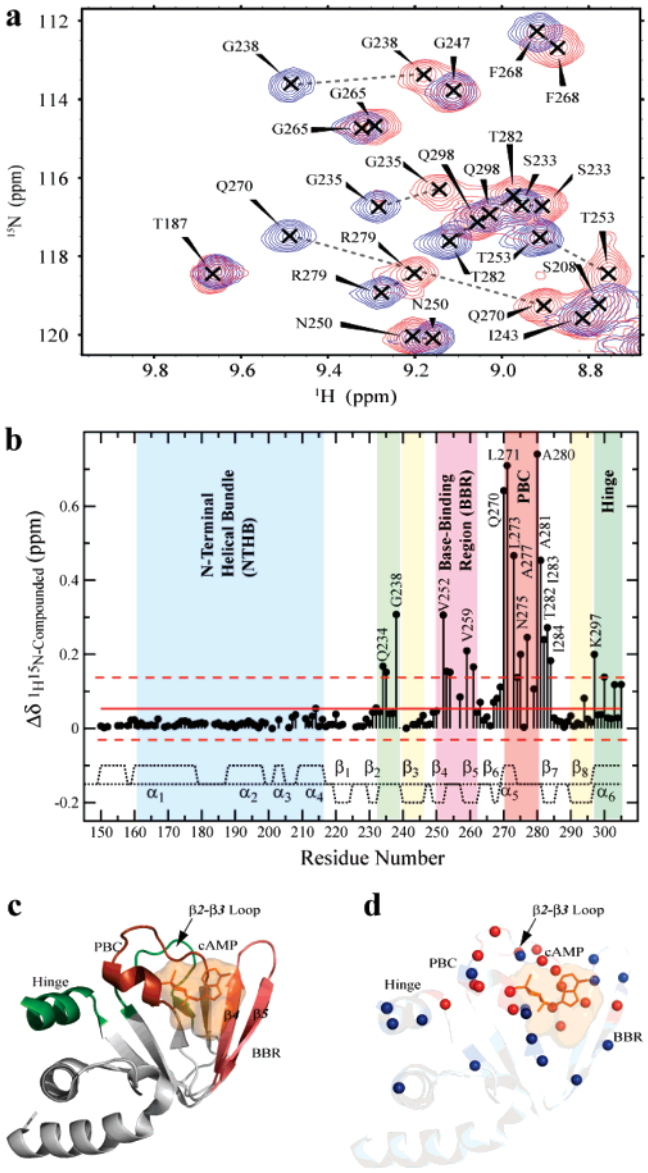

Figure 3. (a) Representative expansion of the ^{1}H−^{15}N-HSQC spectra of 0.5 mM EPAC1$_h$ (149−305) acquired in the absence (red) and presence (blue) of 2 mM excess cAMP. All spectra were recorded at 700 MHz, 34 °C, and pH 7.6 in 50 mM HEPES, 50 mM NaCl, 1 mM TCEP, 0.02% w/v NaN_3 using a Bruker TCI cryo-probe. (b) Compounded ^{1}H,^{15}N chemical shift differences between apo and cAMP-bound EPAC1$_h$ (149−305) plotted against the residue number. The red solid and dashed lines indicate the 10% trimmed average ± one standard deviation, respectively. The chemical shift for the A280 residue is down-scaled by a factor of 0.3 to fit it within the same scale as the other ppm variations. Residues for which no data are reported are either ambiguous or proline. The 2° structure derived as in Figure 1c is indicated by black dotted lines. Representative functional regions are annotated and color coded as in Figure 2. (c) Ribbon representation of the cAMP-binding domain (CBD) of EPAC2$_m$ (PDB accession code: 1O7F).[10] Possible cAMP orientations were gauged by superimposing the phosphate binding cassette of EPAC2$_m$ to those of the following cAMP-bound CBDs: PKA isoform Iα of the R subunit of PKA (RIα) CBD-A (stick representation), HCN, CNG, and CAP with PDB accession codes 1RGS,[7] 1Q43,[53] 1VP6,[54] and 2CGP,[55] respectively. The cAMP van der Waals surfaces are shown for all of the cAMP ligands of these PDB files. Functional regions with significant chemical shift variations are color coded as in panel (b). BBR and PBC stand for "base-binding region" and "phosphate binding cassette", respectively. (d) Same as panel (c), but with the residues subject to significant cAMP-dependent ppm variations marked by balls. Red balls denote sites with compounded chemical shift variations larger than the average + one standard deviation, while blue balls indicate residues with ppm changes between the average and the average + one standard deviation.

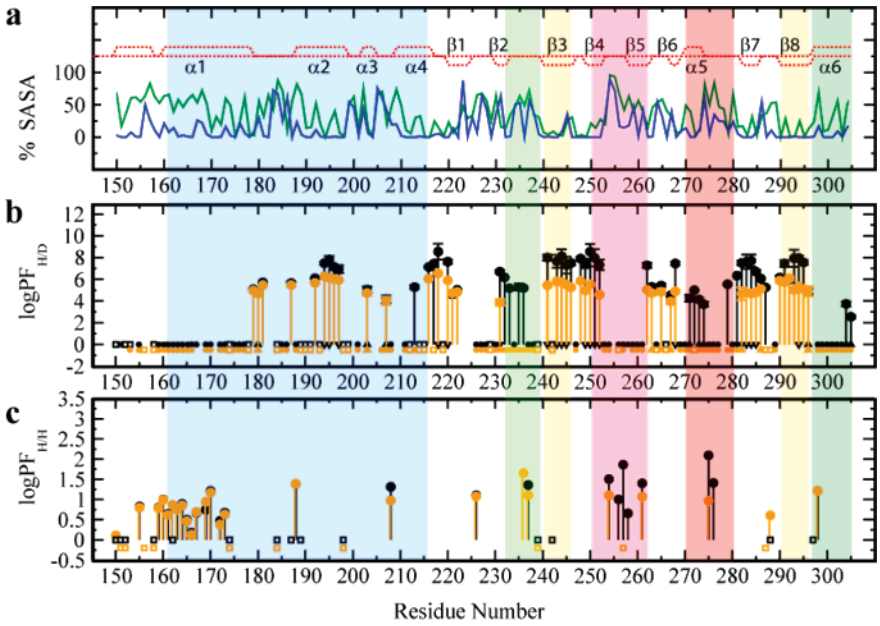

Figure 4. Plot of solvent accessibilities in EPAC1$_h$ (149−305). (a) Plot of the relative residue accessibility calculated as the % ratio of the solvent-accessible surface area (SASA) over the SASA of that residue type in an extended Ala-Xxx-Ala tripeptide. The % SASA was computed for apo EPAC1$_h$ (149−305) (green and blue) using a structure modeled based on the sequence homology to EPAC2$_m$ (Figure 1c). The green line refers to the total (i.e., side-chain + backbone) % SASA, while the blue plot reports the backbone only % SASA. Similar SASA plots (Figure S3) are obtained using the PBD coordinates 1O7F for the X-ray structure of apo EPAC2$_m$.[10] The red dotted lines have the same meaning as in Figure 2b. (b) H/D-exchange-based protection factors (PFs) of cAMP-bound (black) and apo (orange) of 0.25 mM EPAC1$_h$ (149−305). All other experimental conditions are as described in the caption of Figure 3. The filled symbols close to the zero line represent residues for which quantitative H/D exchange rates could not be measured due to fast exchange within the dead time (∼20 min) of the experiment or the acquisition time of the second to third HSQC spectra recorded after exposure to D_2O. Up and down pointing arrows indicate that the reported PF value is a lower or upper limit, respectively. The other open symbols denote residues affected by overlap. Residues for which no data are reported could not be assigned or are prolines. (c) H/H-exchange-based protection factors (PFs) of cAMP-bound (black) and apo (orange) 0.2 mM EPAC1$_h$ (149−305). All other experimental conditions are as described in the caption of Figure 3. Squares have the same meaning as in panel (b). Residues 256, 258, and 276 are ambiguous in the apo form. The annotations and the color coding of the functional regions are as in Figure 2.

in the millisecond to 100 ms time scale.[44,45] The H/H and H/D methods are therefore complementary to each other.

The apo EPAC1$_h$ (149−305) H/D and H/H exchange profiles are reported in Figures 4b and c, respectively. Figure 4a shows the corresponding relative solvent-accessible surface area (SASA) values, with separate plots for the backbone and all-atom (i.e., backbone + side-chain) contributions. While backbone SASA values are a key determinant of the degree of amide protection from solvent exchange, the all-atom SASA is useful to assess whether a given amide is part of a highly buried structural moiety. For instance, for most residues at the N-terminus and at the center of α1 helix, the all-atom SASA values are significantly higher than those for the backbone only SASA (Figure 4a), pointing to an overall highly solvent-exposed helix. Consistently with this observation, most α1 amides exchange fast in the H/D time-scale (Figure 4b) and they are sensed by H/H methods (Figure 4c). Conversely, the inner strands of the β-barrel (i.e., β3, β4, β7, and β8) are characterized by low values for both backbone and all-atom SASAs (Figure 4a), and in agreement with this SASA pattern the corresponding H/D-based protection factors are high (Figure 4b) and no H/H peak was observed (Figure 4c). While in general most of the CBD residues of apo EPAC1$_h$ (149−305) with minimal all-atom SASA values are characterized by maximal protection factor values (i.e., log(PF) ≥ 5), this is however not always the case for the residues in the PBC, in the hinge helix (i.e., α6), and in the β2−β3 loop (Figure 4b,c).

Despite the fact that the apo EPAC crystal structure predicts low solvent accessibility for several amino acids at these three sites (Figure 4a), the apo state H/D exchange rates are mostly fast, indicating only very modest shielding from the solvent and suggesting that the PBC, the α6 helix, and the β2−β3 loop are subject to significant local unfolding fluctuations prior to cAMP binding. Upon cAMP-binding a dramatic increase in protection factors is observed for several residues at these loci (Figure 4b,c), pointing to an at least partial quenching of such local fluctuations. For instance, a remarkable case is that of the amide of D236, which is located between β2 and β3. The D236 NH in the apo state is detected in the H/H CLEANEX spectra, implying exchange in the ∼millisecond time-scale, but after cAMP binds its exchange rate is reduced by more than 2 orders of magnitude (Figure 4b,c). Interestingly, despite the significant cAMP-dependent protection enhancement observed for the PBC, the α6 helix, and the β2−β3 loop (Figure 4b,c), their PF values remain considerably lower than the maximal PFs observed for the cAMP-bound state of EPAC1$_h$ (149−305) (i.e., log(PF$_{Max}$) ≈ 8). This observation suggests that residual local fluctuations to exchange-competent states are still present even in the cAMP-bound state for the PBC, the α6 helix, and the β2−β3 loop. On the contrary, the residues characterized by maximal PF values (Figure 4b) rely on transient global unfolding events for accessing exchange-competent conformers, and the increase of their PFs in the presence of cAMP reflects an overall stabilization of the EPAC CBD upon cAMP-binding.

Discussion

Significance of the EPAC1$_h$ (149−305) Construct. The EPAC1$_h$ construct analyzed in this investigation (Figure 1b) does

not contain the (306−318) segment, which was suggested to possibly serve as a "lid" for the cAMP-binding site based on comparative structural analyses of other cAMP-binding proteins (i.e., PKA, CAP, and HCN).[6,21] However, multiple independent lines of evidence indicate that such a lid region does not significantly affect cAMP-recognition. First, extensive point mutations in the lid region did not perturb appreciably the K_D for cAMP (i.e., the E308A, T311A, R313A, and H317A single mutants result in K_D values in the 4−6 μM range, comparable to the 3 μM K_D reported for the WT).[22] Second, recent molecular dynamics simulations show that H317 does not stack against cAMP in EPAC1,[13] consistently with the similar affinities toward cAMP measured for the H317A and WT proteins.[22] Third, saturation-transfer difference (STD)-based binding studies (Figure 1f) indicate that the affinity of cAMP for $EPAC1_h$ (149−305) is comparable to that for full-length $EPAC1_h$.[13] Fourth, the relevance of the $EPAC1_h$ (149−305) construct is also supported by earlier observations that deletion of the DEP domain at the CBD N-terminus (Figure 2b) has no effect on the cAMP-dependent activation of EPAC.[19,20,24] Fifth, the deletion at the CBD C-terminus of the whole catalytic region of EPAC has been shown not to alter the CBD fold.[10,11] Hence, the $EPAC1_h$ (149−305) construct is expected to be a useful model system to start investigating how the cAMP signal propagates from its binding site to the ionic latch and to other regions within the EPAC CBD.

cAMP Docking into the Phosphate Binding Cassette (PBC) and the Base Binding Region (BBR) of EPAC. The major chemical shift variations observed for the PBC reflect not only the formation of cAMP:EPAC contacts, but also significant conformational rearrangements at the level of the PBC, as indicated by the corresponding cAMP-induced alterations in the secondary structure probabilities (Figure 2a−c) and in the solvent accessibilities (Figure 4b,c). Figure 2a shows that, while cAMP does not alter the overall α/β fold of the EPAC CBD, cAMP binding results in a significant stabilization of the α5 helix within the PBC (Figure 2b) as well as of the β6 and β7 residues adjacent to the PBC, such as F268 and A280, respectively (Figure 2c). The enhanced stability of the PBC and of the neighboring residues is also independently confirmed by an overall increase in shielding from the solvent in these regions (Figure 4b,c). The increased α5 stability in the presence of cAMP is consistent with the presence of charge−dipole interactions and/or with a cAMP-mediated N-terminal capping of α5. In either case, the phosphate of cAMP is positioned at the N-terminus of α5, and the analysis of the known CBD structures[7,8,53−55] shows that such positioning of the cAMP phosphate results in the cAMP adenine being invariably in the vicinity of the β4−β5 region (Figure 3c). In agreement with this observation and with the aromatic ring current contributions arising from the adenine base, several cAMP-dependent chemical shift changes are observed for residues in the β4−β5 segment (Figure 3b,d). Overall our results indicate therefore that the cAMP binding site of EPAC includes both the PBC and the base binding region (BBR), jointly defined by the surfaces of strands β4 and β5 (Figure 3c).

(53) Zagotta, W. N.; Olivier, N. B.; Black, K. D.; Young, E. C.; Olson, R.; Gouaux, E. *Nature* **2003**, *425*, 200−205.
(54) Clayton, G. M.; Silverman, W. R.; Heginbotham, L.; Morais-Cabral, J. H. *Cell* **2004**, *119*, 615−627.
(55) Passner, J. M.; Steitz, T. A. *Proc. Natl. Acad. Sci. U.S.A.* **1997**, *94*, 2843−2847.

cAMP-Dependent Perturbations Beyond the cAMP Binding Site. Multiple lines of evidence consistently point to the presence of several cAMP-dependent long-range effects that propagate well beyond the immediate cAMP binding site (i.e., the PBC and the BBR). First, significant cAMP-induced chemical shift changes are detected for both the β2−β3 loop and the α6 helix (Figure 3b). Such ppm variations cannot be accounted for by direct cAMP contacts or aromatic ring current shifts and reflect therefore genuine cAMP-dependent allosteric perturbations. Second, several residues in these very same regions, that is, the β2−β3 loop and the α6 helix, display a remarkable enhancement in shielding from the solvent upon cAMP-binding to an extent comparable to that observed for the PBC (Figure 4b,c), where the phosphate and ribose moieties of cAMP dock. Third, the secondary chemical shifts (Figure 2a−c) indicate that cAMP binding results in the stabilization of both the β2 strand and the α6 helix. The β2−β3 and the α6 regions emerge therefore as two key allosteric "hot-spots" for the propagation of the cAMP signal.

Our comparative NMR analyses also show that the cAMP signal propagates even beyond the β2−β3 and the α6 regions to the N-terminal helical bundle (NTHB), including the α2−α4 helices. For instance, the secondary chemical shift changes observed upon cAMP-binding point to a significant cAMP-dependent change in helicity at the level of α3 (Figure 2b) located at the center of the NTHB, implying a perturbation in the helical packing of the NTHB. This result is supported by the overall higher degree of protection from solvent exchange observed for α2 and α4 in the cAMP-bound state relative to the apo form (Figure 4b). For instance, several highly buried residues at the C-termini of α2 and α4 (Figure 4a) display an increase in protection factors (PFs) by at least 1 order of magnitude (Figure 4b). Such a change is part of an overall cAMP-induced PF enhancement observed for the inner core residues located not only at the C-termini of α2 and α4 but also in most of the β-strands, with four major clusters confined to the internal β-barrel strands, that is, β3, β4, β7, and β8 (Figure 4a,b). This group of highly buried sites with maximal PFs relies on transient global unfolding hydrogen-exchange pathways, as opposed to local conformational fluctuations to exchange-competent states, and it is therefore expected to respond concertedly to the stabilization resulting from cAMP-binding.

Based on the above discussion, it is clear that the cAMP-signal propagates well beyond the immediate cAMP-binding site, defined by the PBC and the BBR, to several allosteric loci that include not only the β2−β3 loop and the α6 helix, but also the inner CBD core and the N-terminal helical bundle. The latter contains the ionic latch residues (Figure 1c) that mediate key contacts between the regulatory and catalytic regions of EPAC in the apo-state and have been hypothesized to be critical for the activation of EPAC.[10] The next step is therefore to define the cAMP-dependent interaction networks, the EPAC CBD intramolecular signaling pathways that propagate the cAMP-signal from the cAMP-binding site to the ionic latch, through the multiple distal allosteric sites revealed by our comparative NMR analyses. For this purpose, the 2D contact map displayed in Figure 5a is particularly useful. Figure 5a shows that, while no clusters of direct contacts are observed between the PBC or the BBR and the N-terminal helical bundle (NTHB), several indirect pathways from the PBC to the NTHB are possible,

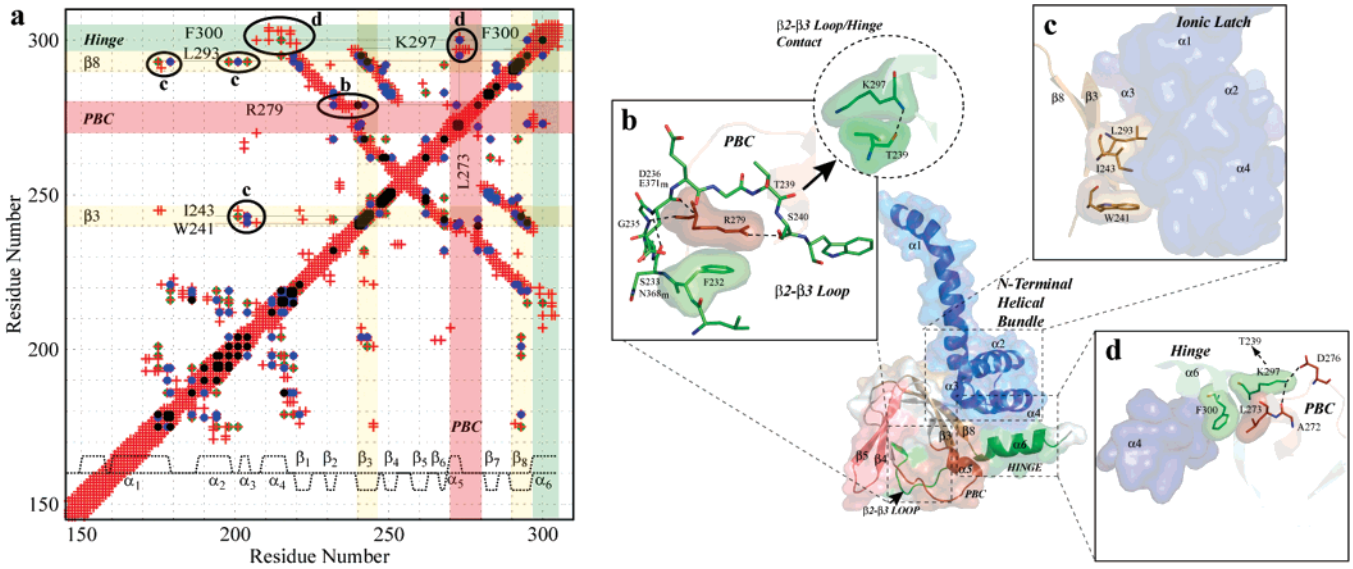

Figure 5. Contact map analysis (a) and a model for the cAMP-dependent intramolecular allosteric signaling pathways in the EPAC CBD (b−d). (a) 2D contact map of $EPAC1_h$ (149−305). Red crosses indicate a contact between two residues with at least two atoms closer than 5 Å. Black, blue, and green filled circles represent contacts between two residues with relative SASAs < 15% and with at least two atoms closer than 3, 4, and 5 Å, respectively. Representative contacts suggested to be critical for the allosteric cross-talk between the PBC and the N-terminal helical bundle are labeled and highlighted by black ovals. Also indicated are the corresponding panels in this figure where these contacts are illustrated. The 2° structure is shown in the bottom similarly to Figure 2b. The contact map was computed using the coordinates of the homologous $EPAC2_m$ (PDB access code 1O7F).[10] (b) Interactions mediating the communication between the $\beta2-\beta3$ loop and the PBC R279. The circular inset shows the contacts between the $\beta2-\beta3$ loop and the hinge (α6) region. (c) Contacts between the adjacent strands $\beta3$, $\beta8$ and the N-terminal helical bundle, where the ionic latch is located. (d) Interactions mediating the communication between the hinge helix, the PBC, and helix α4. In panels (b−d), residues that are conserved between $EPAC1_h$ and $EPAC2_m$ are labeled according to the $EPAC1_h$ residue numbers, whereas for nonconserved residues an additional label appears with the $EPAC2_m$ residue name and number and the subscript m. The color coding of the different functional regions is as in Figure 2. These figures were prepared using the coordinates of the homologous $EPAC2_m$ (PDB access code 1O7F).[10]

provided that the interactions with the $\beta2-\beta3$ loop and the α6 helix allosteric relay sites are considered. In the following sections, both the α6 and the $\beta2-\beta3$-mediated cAMP-signaling pathways will be examined.

Defining the Intramolecular Signaling Pathways Mediated by the α6 Hinge Helix. The contact map of Figure 5a shows that the cAMP-dependent chemical shifts and secondary structure changes observed for the N-terminus of α6 (Figures 3b and 2a,b) are fully consistent with two possible sets of contacts between the PBC and α6. The first set involves the conserved L273 of α5 and F300 of α6, as previously proposed.[11] Furthermore, it should be noted that L273 and F300 are part of a hydrophobic cluster that includes also the aliphatic portion of K297 found at the N-terminus of α6 (Figure 5a,d), which in turn forms a second set of interactions with the PBC whereby the K297 amino group donates a hydrogen bond to the carbonyl oxygen of A272 and forms a salt bridge with the carboxylate of D276 (Figure 5d). Considering that both A272 and D276 are part of the PBC, it appears that the cross-talk between the PBC and α6 results from a combination of steric hindrance between hydrophobic side-chains (i.e., L273, F300)[11] and of polar/ionic interactions (i.e., A272, D276, and K297; Figure 5d), suggesting that not only F300 but also K297 is a key allosteric residue within α6. This conclusion is supported by the observation that the cAMP-dependent changes in the compounded ^1H and ^{15}N chemical shifts and in the α-helix probability measured for K297 are comparable or larger than those reported for F300 (Figures 3b and 2b).

A fuller appreciation of the K297 and F300 function is obtained by analyzing the other interactions mediated by these loci. The contact map analysis (Figure 5a) reveals that the α6 residues K297 and F300 play a pivotal role not only in the α6-PBC cross-talk, but also in relaying the cAMP-signal to other critical allosteric sites of the EPAC CBD, such as the $\beta2-\beta3$ region and the N-terminal helical bundle, respectively (Figure 5a). Specifically, K297 interacts with T239 at the N-terminus of $\beta3$ both through its methylenes, which are in close van der Waals contact with the T239 Cβ and Cγ, and through its amide, which donates a hydrogen bond to the carbonyl of T239 (Figure 5b). Unlike K297, F300 forms through its side-chain multiple contacts with α4 (Figure 5a,d), accounting for the cAMP-dependent changes in protection factors observed for α4 (Figure 4b,c) and defining an α6-mediated intramolecular pathway that propagates the cAMP signal from the PBC to the N-terminal helical bundle (NTHB). However, the one mediated by α6 is not the only allosteric network for the cross-talk between the PBC and the NTHB. For instance, another possible PBC-to-NTHB pathway is relayed by the $\beta2-\beta3$ loop, as shown by the contact map in Figure 5a.

Defining the Intramolecular Signaling Pathways Mediated by the $\beta2-\beta3$ Loop. A possible set of interactions that accounts for the marked cAMP-dependent changes in chemical shifts, 2° structure, and solvent shielding observed for the $\beta2-\beta3$ loop (Figures 3b, 2a,c, and 4b,c) involves both the backbone and the side-chain of one of the most conserved residues in the PBC, that is, R279 (Figure 5b). As shown in Figure 5b, the backbone of R279 hydrogen bonds the carbonyl of D236 through its amide and the amide of G235 through its carbonyl. G235 is located at the center of a β-turn stabilized by a hydrogen bond between the amide of D236 and the carbonyl of S233 (Figure 5b). As a result, all three amides of R279 in the PBC, and of G235 and of D236 in the $\beta2-\beta3$ loop, are involved in backbone-to-

backbone hydrogen bonds, and the hydrogen-exchange data show that the solvent shielding caused by such hydrogen bonds is dramatically enhanced by cAMP-binding (Figure 4b,c), suggesting that only in the presence of cAMP this extended interaction network involving both the PBC and the $\beta2-\beta3$ loop is fully nucleated.

The critical role of the buried PBC R279 is not limited to its backbone but it involves also its side-chain, which contacts through its methylenes the aromatic ring of F232 at the C-terminus of $\beta2$ and through its guanidinium the backbone of S240 at the N-terminus of $\beta3$ (Figure 5b). The latter residue is adjacent to T239, which in turn connects the $\beta2-\beta3$ loop to the $\alpha6$ helix through its interactions with K297, as discussed above (Figure 5a,b). Because of this set of interactions that radiate out of R279, the perturbation caused by cAMP-binding on this conserved PBC arginine is propagated to the highly buried F232 and S240, respectively located at the C- and N-termini of $\beta2$ and $\beta3$, as well as to T239. This result is confirmed by the increased protection factor observed for F232 in the presence of cAMP (Figure 4b) and by the significant variation in β-strand probability occurring for T239 upon cAMP-binding (Figure 2c). Such cAMP-dependent perturbations of $\beta2$ and $\beta3$ propagate also to the adjacent $\beta8$ (Figures 4b and 5a,c) and possibly to other residues of the inner CBD core, which, as discussed above, respond to cAMP in a concerted manner. Within such a highly buried and cAMP-sensitive ensemble, $\beta3$ and $\beta8$ are the internal strands of the β-barrel side facing the N-terminal helical bundle (NTHB) and include several residues, such as W241, I243, and L293, that interact extensively with $\alpha3$ (Figure 5a,c). This allosteric interaction network is supported by the major cAMP-dependent variations in α-helix probability observed for $\alpha3$ (Figure 2b) and defines a $\beta2-\beta3$-mediated pathway that relays the cAMP signal from the PBC to the NTHB, which includes the IL.

Comparison between the CBDs of PKA and of EPAC. The picture of the EPAC CBD allosteric networks revealed in this investigation shows that the key "hot-spots" of the CBD allostery are analogous in PKA[12] and EPAC, as both systems rely on the "cross-talk" between the cAMP-binding site, comprising the PBC and the BBR, the hinge helix, the $\beta2-\beta3$ region, and the NTHB. However, the nature of the communication among these allosteric elements is somewhat different in EPAC and PKA. Most strikingly, all of the detectable amides within the NTHB of the PKA CBD-A are subject to rapid exchange with the solvent,[12] while in the EPAC CBD several NTHB residues are well-shielded from the solvent (Figure 4b), pointing to a tighter packing of the NTHB helices in EPAC as compared to PKA. Most notably, the protection factors measured in the C-terminal regions of $\alpha2$ and $\alpha4$ are among the highest observed within the whole EPAC CBD and are subject to the cAMP-dependent control of global unfolding exchange pathways. It is possible that the stability of the EPAC NTHB has survived evolutionary selection as it is functional to the effective propagation of the cAMP-signal from the PBC/BBR region to the IL sites within the NTHB, which are critical for the activation of EPAC. In other words, the class of highly buried residues that is subject to global unfolding H/D exchange pathways and that is characterized by a concerted collective response to cAMP-binding is significantly more extended in EPAC than in PKA. In PKA these highly buried residues are confined mostly to the β-subdomain, while in EPAC they extend also to selected regions of the N-terminal α-helical subdomain, resulting in a tighter inter-subdomain coupling. Another major difference between the EPAC and PKA CBDs concerns the interactions that couple the PBC and the C-terminal hinge helix (i.e., labeled as $\alpha6$ in EPAC and as B-helix in PKA, Figure S1). While the comparative NMR study presented here supports the hypothesis that the L273/F300 pair is a key determinant of the PBC/$\alpha6$ "cross-talk" in EPAC, in PKA point mutations at the corresponding sites (i.e., L203 and Y229) have shown that the allosteric role played by this hydrophobic contact is not as critical as in EPAC.[56]

Conclusions

The identification of an $EPAC1_h$ CBD construct that is stable and suitable for NMR investigations in both its apo and its cAMP-bound forms has revealed at an unprecedented level of detail several allosteric features for the activation of EPAC, and possibly of other cAMP-regulated systems. Specifically, the combined analysis of the cAMP-dependent changes in chemical shifts, secondary structure probabilities, H/H and H/D protection factors has unveiled that: (a) cAMP binding perturbs the PBC by stabilizing the adjacent $\beta6$ and $\beta7$ residues and the $\alpha5$ helix, consistently with phosphate charge−helix dipole and/or N-terminal capping interactions mediated by cAMP; and (b) two distinct intramolecular cAMP-signaling pathways propagate the perturbation caused by cAMP on the PBC to the other critical distal functional site of the EPAC CBD, that is, the NTHB, where the ionic latch connecting the regulatory and catalytic regions of EPAC is located. One pathway is mediated by the $\beta2-\beta3$ loop and affects primarily the $\alpha3$ and possibly the $\alpha1$ helices of the NTHB. The other is mediated by $\alpha6$ and controls mostly the $\alpha4$ NTHB helix. Both pathways account for the observed cAMP-dependence of the NTHB inner core packing, even in the absence of direct PBC/NTHB contact clusters. Such cAMP-dependent variations in the NTHB provide a possible rationalization for how cAMP-binding weakens the ionic latch that secures the regulatory region of EPAC to its catalytic counterpart and sterically inhibits access to EPAC substrates. The cAMP-triggered weakening of the ionic latch allows the cAMP-dependent perturbation at the PBC/$\alpha6$ sites to drive the displacement of the EPAC CBD away from the catalytic domain, which then becomes accessible to EPAC substrates.[6] This mechanism based on the cAMP-dependent IL release and on the CBD rigid body movement provides a possible explanation for how cAMP activates EPAC.[6] While such a model relies on two distinct intramolecular cAMP pathways mediated by $\beta2-\beta3$ and by $\alpha6$, it is possible that these allosteric networks may act in a concerted manner as suggested by the interactions between T239 and K297 at the N-termini of $\beta3$ and $\alpha6$, respectively. In either case, our results suggest that the previously proposed cAMP-dependent L273/F300 contact should be considered as part of a significantly more extended allosteric interaction network that affects both the α- and the β-subdomains of the EPAC CBD. It is possible that such intramolecular signaling pathways may propagate even beyond the EPAC CBD to other functional sites, such as the so-called switchboard region C-terminal to the CBD; however, longer EPAC constructs will be required to investigate further this hypothesis in the future.

(56) Vigil, D.; Lin, J. H.; Sotriffer, C. A.; Pennypacker, J. K.; McCammon, J. A.; Taylor, S. S. *Protein Sci.* **2006**, *15*, 113−121.

Our study has also revealed a clear difference between PKA and EPAC at the level of their inter-subdomain couplings. In addition, we anticipate that the proposed comprehensive model for the activation of EPAC by cAMP will serve as a basis to understand agonism and antagonism[57,58] in this critical cAMP-sensing domain, opening new opportunities in the pharmacological modulation of cAMP-controlled conformational switches. Furthermore, the mechanism of allosteric activation by cAMP offers a prototype for how small ligands control protein/protein interfaces in general.[59]

(57) Das, R.; Melacini, G. *J. Biol. Chem.* **2007**, *282*, 581−593.
(58) Dostmann, W. R. G. *FEBS Lett.* **1995**, *375*, 231−234.
(59) Kern, D.; Zuiderweg, E. R. P. *Curr. Opin. Struct. Biol.* **2003**, *13*, 748−757.

Acknowledgment. We are grateful to Dr. Xiaodong Cheng for generously providing the $EPAC1_h$ cDNA and, together with Dr. Susan S. Taylor and Dr. Mona Abu-Abed, for helpful discussions. This project was supported by the Canadian Institutes of Health Research (CIHR). G.M. thanks the Heart and Stroke Foundation of Canada (HSFC) for a Maureen Andrew New Investigator Award.

Supporting Information Available: Further details on sequence alignment, binding, and SASA data. This material is available free of charge via the Internet at http://pubs.acs.org.

JA0753703